Enhancing Proteotoxic Stress in Leiomyosarcoma Cells Triggers Mitochondrial Dysfunctions, Cell Death, and Antitumor Activity *in vivo*

Luca Iuliano[1], Sara Drioli[2], Ymera Pignochino[3,4], Claudia Maria Cafiero[2], Martina Minisini[1], Francesca D'Este[1], Raffaella Picco[1], Emiliano Dalla[1], Giorgia Giordano[4,5], Giovanni Grignani[4], Eros Di Giorgio[1], Fabio Benedetti[2], Fulvia Felluga[2], and Claudio Brancolini[1]

ABSTRACT

Leiomyosarcomas are rare and aggressive tumors characterized by a complex karyotype. Surgical resection with or without radiotherapy and chemotherapy is the standard curative treatment. Unfortunately, a high percentage of leiomyosarcomas recurs and metastasizes. In these cases, doxorubicin and ifosfamide represent the standard treatment but with low response rates. Here, we evaluated the induction of proteotoxic stress as a possible strategy to kill leiomyosarcoma cells in a therapeutic perspective. We show that aggressive leiomyosarcomas coexist with high levels of proteotoxic stress. As a consequence, we hypothesized that leiomyosarcoma cells are vulnerable to further increases of proteotoxic stress. The small compound 2c is a strong inducer of proteotoxic stress. In leiomyosarcoma cells, it triggers cell death coupled to a profound reorganization of the mitochondrial network. By using stimulated emission depletion microscopy, we have unveiled the existence of DIABLO/SMAC clusters that are modulated by 2c. Finally, we have engineered a new version of 2c linked to polyethylene glycol though a short peptide, named 2cPP. This new prodrug is specifically activated by proteases present in the tumor microenvironment. 2cPP shows a strong antitumor activity *in vivo* against leiomyosarcomas and no toxicity against normal cells.

Introduction

Leiomyosarcomas (LMS) are rare and aggressive tumors that show some smooth-muscle features and represent approximately 10% of soft-tissue sarcomas (STS) of adults. Leiomyosarcomas are characterized by high mutational burden and a complex karyotype (1, 2). Recent progresses in genomic studies have provided a better classification of STS, including leiomyosarcomas and outlined the complex pattern of mutations (3–5).

The therapeutic perspectives for advanced leiomyosarcomas have not improved during the last decades. Available treatments are surgery and radiotherapy. Unfortunately, local recurrence and metastasis occur in approximately 40% of patients (2). Since the 1970s, doxorubicin is the first-line treatment with few additional options (6). Recently, some hopes have been raised by olaratumab, a human mAb that inhibits the PDGF receptor-α. Disappointingly, a phase III clinical trial in patients with advanced STS, including several leiomyosarcomas, did not evidence significant differences in overall survival after treatment with doxorubicin plus olaratumab versus doxorubicin plus placebo (7). Hence, new therapeutic approaches are urgently needed.

An unbalanced proteostasis triggers proteotoxic stress and, if unresolved, leads to cell death (8). In general, cancer cells present higher levels of proteotoxic stress. The increased metabolic and proliferative rates require elevated levels of protein synthesis, a process prone to errors (9). They are also more exposed to reactive oxygen species (ROS) and starvation, which can cause protein misfolding (8, 10). Aneuploidy, copy-number alterations, and the accumulation of point mutations in coding sequences are additional sources of proteotoxic stress (10–12). Cancer cells coexist with an increased level of proteotoxic stress by upregulating mechanisms counteracting protein misfolding including chaperones, the ubiquitin-proteasome system, and macroautophagy. As a consequence, cancer cells show an enhanced vulnerability to a further increase of proteotoxic stress and are more prone to die (10). Therefore, a new therapeutic option could be the exploitation of small molecules capable of triggering proteotoxic stress (13–15). In this article, we augmented the proteotoxic stress in leiomyosarcoma cells to elicit cell death. We used the small molecule 2c, a diaryldienone derivative, which is a well-known inducer of proteotoxic stress. These compounds make covalent adducts with free thiols by Michael addition (16, 17). In a therapeutic perspective, we have also engineered a new prodrug version of 2c that is activated in the tumor microenvironment after proteolytic cleavage.

Materials and Methods

Cell culture conditions, drug treatments, and propidium iodide staining

Leiomyosarcoma cell lines (SK-UT-1, SK-LMS-1, and DMR) were validated by RNA profiling and grown as described previously (18). The primary human uterine smooth-muscle cells (HUtSMCs) were obtained from ATCC and used within eight passages. All cell lines were weekly tested to be free from *Mycoplasma* contamination using

[1]Department of Medicine, Università degli Studi di Udine, Udine, Italy. [2]Dipartimento di Scienze Chimiche e Farmaceutiche, Università degli Studi di Trieste, Trieste, Italy. [3]Department of Clinical and Biological Sciences, University of Torino, c/o San Luigi Gonzaga Hospital, Orbassano, Torino, Italy. [4]Sarcoma Unit, Division of Medical Oncology, Candiolo Cancer Institute, FPO-IRCCS, Candiolo, Torino, Italy. [5]Department of Oncology, University of Torino, Torino, Italy.

Note: Supplementary data for this article are available at Molecular Cancer Therapeutics Online (http://mct.aacrjournals.org/).

Corresponding Author: Claudio Brancolini, Department of Medicine, Università di Udine, P. le Kolbe 4, Udine 33100, Italy. Phone: 39 043 249 4381; E-mail: claudio.brancolini@uniud.it

Mol Cancer Ther 2021;XX:XX–XX

doi: 10.1158/1535-7163.MCT-20-0521

Hoechst 33258 (Sigma) staining and microscopic inspection. For propidium iodide (PI) staining, cells were collected and resuspended in 0.1 mL of PBS and incubated with 10 μg/mL of PI (Merck), for 5 minutes at room temperature. PI fluorescence positivity was determined with Countess II FL automated cell counter (Invitrogen).

Mutation rate and genomic alteration analysis

The Cancer Genome Atlas (TCGA) tumor mutation counts based on exome-sequencing data, as well as information on the fraction of genome altered (FGA) defined by SNP arrays, were downloaded from cBioPortal (19). We analyzed the whole Sarcoma dataset (TCGA, PanCancer Atlas; $n = 255$) and within this dataset the patients with leiomyosarcoma ($n = 100$; ref. 20). From the same repository, we also retrieved the most recently updated matched Cancer Cell Line Encyclopedia (CCLE) samples (21) focusing on leiomyosarcoma cell lines.

Survival analysis

The R/Bioconductor package *cgdsr* was used to retrieve gene expression (RSEM) and clinical data from patients with leiomyosarcoma. The Kaplan–Meier survival analysis was performed considering the median expression value of each gene signature using the R/Bioconductor *survival* package as described previously (22). We used the "optimal" cut-off point to dichotomize the patients. To select the best cutoff, the R/Bioconductor *SurvMisc* package was used (23).

Chemicals, antibodies, and immunoblotting

The following chemicals were used: PI, Ferrostatin-1, Erastin, Thapsigargin, and DMSO (Merck); Bortezomib (LC Laboratories); TNF-related apoptosis-inducing ligand (TRAIL; ref. 24); Boc-D-fmk (Abcam); Necrostatin-1 (Enzo Life Sciences); 17-(Allylamino)-17-demethoxygeldanamycin (17-AAG; Cayman Chemicals). Immunoblotting was performed as described previously (25). After blocking for 1 hour at room temperature, membranes were incubated with the primary antibodies. The primary antibodies used were anti-Actin and NOXA/PMAIP1 (Merck), DIABLO/SMAC (26), HDAC4 (27), Ubiquitin (Covance), eIF2α, and p-eIF2α (Ser51; Cell Signaling Technology). Next, membranes were incubated with the proper horseradish peroxidase–conjugated secondary antibody for 1 hour at room temperature (Merck). Blots were developed using Super Signal West Dura (Pierce Waltham).

RNA extraction and qRT-PCR

Cells were lysed using Tri-Reagent (Molecular Research Center). A total of 1.0 μg of total RNA was retrotranscribed by using 100 units of M-MLV Reverse transcriptase (Life Technologies). qRT-PCRs were performed using SYBR green technology (KAPA Biosystems). Data were analyzed by comparative threshold cycle using *HPRT* and *GAPDH* as normalizer.

Synthesis of 2cPP and other 2c derivatives

Inhibitors 2c and 2cPE were prepared as reported previously (28). DU-DC2 was obtained in a 51% total yield by conversion of 2c into the O-succinimidoyl ester 2c-OSu (28) followed by reaction of the resulting activated ester with b-alanine. DU-MS1 was obtained in three steps and 56% total yield from 2c-OSu: the spacer was introduced first by reaction of the activated ester with 1,3-diaminopropane and the resulting amine was reacted with N-Boc-(L)-leucine under standard peptide coupling conditions (EDC, HOBt). Finally, the Boc protection was removed with trifluoroacetic acid. 2cPP was synthesized in 77% yield with a convergent approach: monomethoxy polyethylene glycol (PEG; 5,000 kDa) was converted into the corresponding succinimidoyl ester and this compound was reacted with b-alanine giving the PEG-5000-spacer fragment. The Gly-Gly portion was assembled sequentially by reaction of this fragment with glycine benzyl ester, followed by deprotection. The coupling (EDC, HOBt)—deprotection (H2, Pd/C) cycle was repeated twice to introduce the two Gly residues. The PEG-Spacer-Gly-Gly building block thus obtained was finally coupled to DU-MS1 (EDC-HOBt) giving 2cPP. All new compounds had spectral (1H NMR, ESI-MS) data in agreement with the structure. Full details of the syntheses will be reported elsewhere.

Proteases analysis

The list of peptidases was obtained from MEROPS, the peptidase database (https://www.ebi.ac.uk/merops). mRNA expression levels (RSEM data) of the selected peptidases in patients with leiomyosarcomas ($n = 99$) were derived from the Sarcoma dataset [TCGA, PanCancer Atlas; $n = 255$ (20)]. The mRNA expression levels of the selected peptidases in the leiomyosarcoma cell lines were retrieved from the CCLE database (29).

Immunofluorescence confocal and stimulated emission depletion microscopy

For immunostaining, cells grown on No. 1.5 coverslips were fixed with 3% paraformaldehyde (Merck) for 20 minutes at room temperature, quenched with 100 mmol/L glycine for 5 minutes, and permeabilized with 0.5% Triton X-100 for 5 minutes. Nonspecific binding was blocked with 1% BSA (Merck) in PBS for 1 hour at room temperature. Primary and secondary antibody incubations were carried out at 37°C in PBS supplemented with 1% BSA and 0.5% Triton X-100, for 45 and 30 minutes, respectively. The following primary antibodies were used: anti-DIABLO/SMAC [(26), 1:100 dilution]; anti-ATP Synthase β (Thermo Fisher Scientific, catalog No. MA1-930, 1:200 dilution); anti-Cytochrome c (CytC; Thermo Fisher Scientific, catalog No. 33-8200, 1:100 dilution). Secondaries included Alexa Fluor 532–conjugated anti-mouse (catalog No. A11002) and anti-rabbit (catalog No. A11009) antibodies, and Alexa Fluor 568–conjugated anti-mouse (catalog No. A11019) and anti-rabbit (catalog No. A21069) F(ab')2 fragments (Thermo Fisher Scientific, 1:100 dilution). Coverslips were mounted in Mowiol (Merck) supplemented with 2.5% DABCO (Merck).

Comparative confocal and stimulated emission depletion (STED) images were acquired on a Leica TCS SP8 STED confocal microscope (Leica Microsystems) equipped with a pulsed white-light excitation laser, a 660-nm STED depletion laser, HC PL APO CS2 100×/1.40 oil objective and time-gated hybrid detectors. Excitation was carried out at 514-nm for Alexa Fluor 532 and at 580 nm for Alexa Fluor 568. Signal was detected at 520 to 565 and 590 to 650 nm, respectively. Both fluorophores were depleted using the 660-nm laser. Images from single optical sections were acquired in sequential scanning mode using Leica Application Suite X (LAS X) 3.5.5 software. Contrast was linearly adjusted on the whole image using Adobe Photoshop. Averaged intensity profiles were measured along a 60-nm-wide line using LAS X. Each profile was normalized to its respective peak intensity.

Leiomyosarcoma xenograft tumors in mice

Six-week-old female athymic nude-foxn1nu mice (Envigo Italy) were utilized for SK-UT-1 xenograft experiments. Animal studies were carried out according to the guidelines enforced in Italy (DDL 116 of

Feb 21, 1992 and subsequent addenda) and in compliance with the Guide for the Care and Use of Laboratory Animals, Department of Health and Human Services Publication No. 86-23. *In vivo* xenografts were established from initial subcutaneous injection of SK-UT-1 cells in 12 mice. For DMR xenografts, 2×10^6 DMR cells were embedded in ice-cold 50% growth factor–reduced BD Matrigel TM (BD Biosciences): PBS and subcutaneously injected into the right flank of 6-week-old female NSG mice (Charles River Laboratory). When tumor size was approximately 0.1 cm^3, mice were treated intravenously every 4 days, for three times with 170 mg/kg of 2cPP dissolved in PBS. Before treatment, mice were randomly assigned to experimental groups ($n = 2$ with 6 mice/group). All animals were checked daily, and eventual behavioral changes, ill health, or mortality was recorded for each animal. At the end of the experiments, mice were sacrificed and autopsy was performed on all mice: thoracic and abdominal cavity was open, and all major organs were macroscopically examined. Livers from all animals were collected and weighted.

Statistical analysis

For experimental data, Student *t* test was employed. For comparisons between samples >2, ANOVA test was applied coupled to Kruskal–Wallis and Dunn multiple comparison test. We marked with *, $P < 0.05$; **, $P < 0.01$; ***, $P < 0.001$. Unless otherwise indicated, all the data in the figures were represented as arithmetic means ± the SDs from at least three independent experiments.

Results

Genomic alterations and proteotoxic stress in leiomyosarcomas

Induction of proteotoxic stress can be observed in relation to genomic alterations (10, 11, 12). The overexpression of genes, as well as the accumulation of mutations in coding regions, can alter the normal proteostasis (12, 30). These mutations would produce protein variants that are prone to misfolding, degradation, and aggregation.

To unveil the origin and the extent of proteotoxic stress, we evaluated the FGA in leiomyosarcomas and in STS. FGA is the percentage of genome that has been affected by copy-number gains or losses (31). More than 50% of patients with leiomyosarcomas show a very high percentages of genetic alterations (FGA > 50%). STS groups are a heterogeneous family of tumors that also comprise synovial sarcomas, marked by few genomic alterations. Not surprisingly, FGA is heterogeneous also in STS (**Fig. 1A**). Next, we compared the mutations burden [(mutation counts (MC)] in relation to FGA in leiomyosarcomas and STS (**Fig. 1B** and **C**). The mutations burden is also heterogeneous in leiomyosarcomas, with few cases presenting high MC (>100). Similar heterogeneity is observed in STS where leiomyosarcomas and myxofibrosarcoma comprise cases with the highest MC, whereas synovial sarcomas and dedifferentiated liposarcomas are characterized by lower MC (Supplementary Fig. S1).

Afterward, we evaluated FGA and MC in three leiomyosarcoma cell lines (RKN, SK-LMS-1, SK-UT-1). For comparison, we used fibroblasts as a reference of a normal genome. Interestingly, SK-LMS-1 cells resemble leiomyosarcomas with high FGA and relative low MC. In contrast, SK-UT-1 cells represent leiomyosarcomas, characterized by relative low FGA but high MC (**Fig. 1D**). As reported previously, more mutations are present in the cell lines compared with tissues (31). For the subsequent studies, we selected SK-LMS-1 and SK-UT-1 cells, as models of two different landscapes of genetic alterations observed in leiomyosarcomas.

The small molecule 2c makes covalent adducts with free thiols of cysteines and triggers proteotoxic stress and cell death (16, 17). Gene profile studies performed in B-cell chronic lymphocytic leukemia (B-CLL) have identified, among the early response genes to 2c, several components of the proteotoxic response, including: chaperons, proteasomal subunits, and antioxidants (16). We selected a signature of 38 genes upregulated in B-CLL cells in response to 2c (Supplementary Table S1) to evaluate its dysregulation in leiomyosarcomas. **Figure 1E** shows that this general signature is highly expressed in the subgroup of patients that shows a worse prognosis. We extracted from this general signature a specific signature of 18 genes that collects elements of the proteotoxic response, as defined by the Gene Ontology or by literature (Supplementary Table S1 or Supplementary Table S2). Not surprisingly, the proteotoxic signature comprises several chaperones. Interestingly, patients with reduced survival are characterized by high levels of expression of the 2c proteotoxic stress signature (**Fig. 1F**). Moreover, there is a good correlation between patients with leiomyosarcomas with high MC (>46 $n = 39$) and the expression of the 2c proteotoxic signature ($r = 0.46$; $P = 0.00325$).

2c triggers proteotoxic stress, mitochondrial dysfunctions, and cell death in leiomyosarcoma cells

The previous analysis suggests that aggressive leiomyosarcomas are characterized by high levels of proteotoxic stress. In these tumors, a further increase of protein misfolding could be deleterious for the survival of the neoplastic cells. To investigate this hypothesis, we evaluated the ability of 2c to trigger proteotoxic stress in SK-UT-1 and SK-LMS-1 cells. As a measure of proteotoxic stress induction, the mRNA levels of three chaperones: *HSPA1A, HSPA6*, and *DNAJB6* were analyzed.

The expression levels of *HSPA1A* and *HSPA6* are dramatically upregulated in the two leiomyosarcoma cells in response to 2c. In contrast, *DNAJB6* remains unaffected or slightly decreases (**Fig. 2A**). The induction of 2c-dependent proteotoxic stress is coupled with the appearance of cell death in both cell lines (**Fig. 2B**). This cell death is partially dependent on caspases, as proved by the incomplete effect of the caspase inhibitor (**Fig. 2B**). The combination TRAIL/bortezomib was used as a reference for the caspase-dependent cell death. 2c-induced cell death is unrelated to ferroptosis and only marginally entails necroptosis (Supplementary Fig. S2A). Erastin proved the efficiency of the ferroptosis inhibitor ferrostatin-1 (Supplementary Fig. S2B). To further confirm the induction of proteotoxic stress, cells were cotreated with 2c and the HSP90 inhibitor 17-AAG. The two compounds show an additive pro-death effect, particularly when used at low doses (Supplementary Fig. S2C). The pleiotropic nature of the cell death response elicited by 2c was also observed in previous studies (16, 17, 25, 26).

EC_{50} values for 2c are 4.47 + 1.04 μmol/L in SK-UT-1 and 15.60 + 2.81 μmol/L in SK-LMS-1 cells (Supplementary Fig S2D). The differential sensitivity to proteotoxic stress of the two leiomyosarcoma cells is confirmed by other inducers of proteotoxic stress: the proteasome inhibitor bortezomib and thapsigargin, an inhibitor of the SERCA transport ATPase (10). Both stressors are less potent in SK-LMS-1 cells with EC_{50} values of 32.79 + 0.67 μmol/L (bortezomib) and 33.64 + 0.54 μmol/L (thapsigargin) compared with 23.13 + 0.75 μmol/L and 28.92 + 0.57 μmol/L, respectively, in SK-UT-1 cells. In summary, leiomyosarcoma cells with higher MC are more sensitive to proteotoxic stress.

Cell death in leiomyosarcoma cells is characterized by the upregulation of the BH3-only protein NOXA/PMAIP1 (**Fig. 2C**), a component of the apoptotic pathway elicited by endoplasmic reticulum stress (12). The induction of caspase activity by 2c is verified by the proteolytic processing of death substrate HDAC4 (27). As expected, 2c triggers the

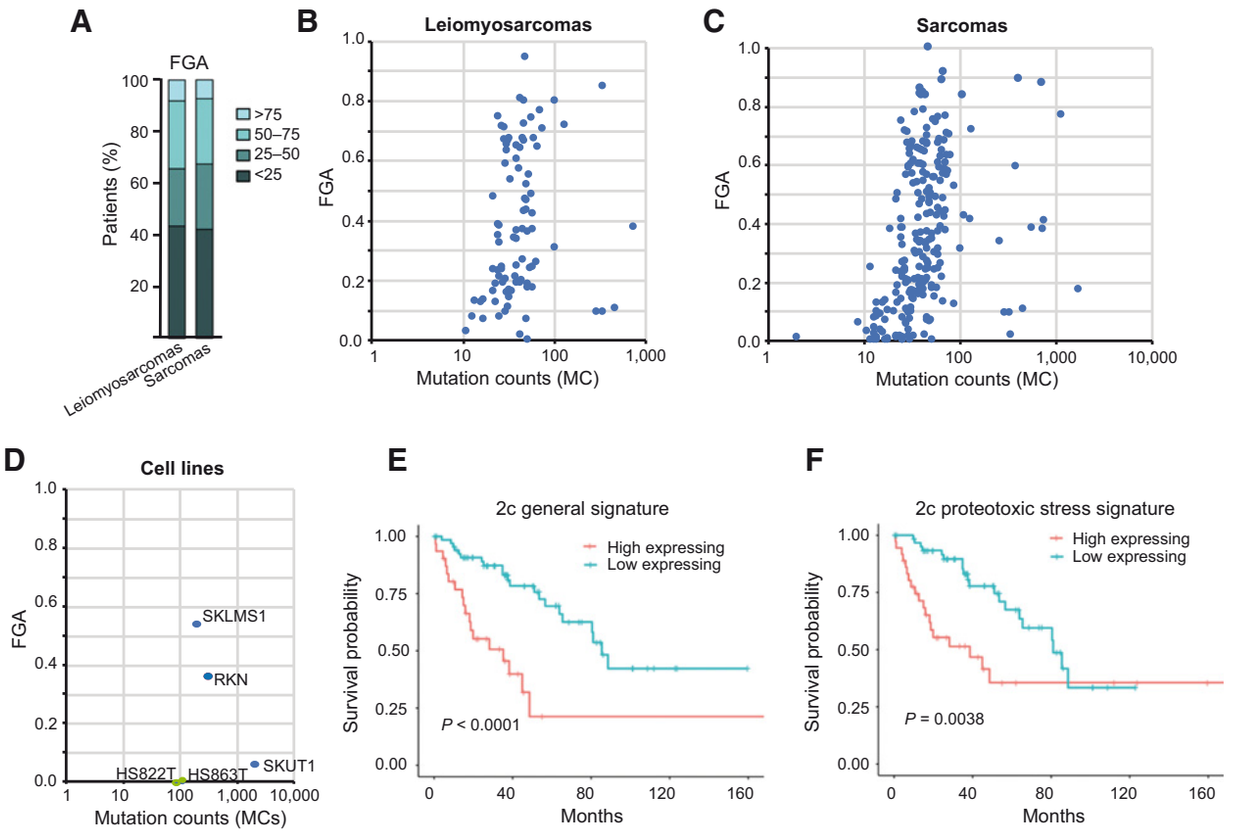

Figure 1.

Analysis of the mutational burden in patients with sarcoma and leiomyosarcoma. **A,** FGA in patients with sarcoma and leiomyosarcoma. Percent stacked bar charts illustrating the distribution of patients with sarcoma ($n = 255$) and leiomyosarcoma ($n = 100$) considering the FGA parameter (patients were divided into four groups based on this value). Data taken from the TCGA-PanCancerAtlas. **B,** Scatter plot showing the FGA and the distribution of MC in patients with leiomyosarcoma ($n = 100$). Data taken from TCGA-PanCancerAtlas. **C,** Scatter plot showing the FGA and the distribution of MC in patients with sarcoma ($n = 255$). Data taken from TCGA-PanCancerAtlas. **D,** Scatter plot of FGA and MC distribution in human fibroblasts and leiomyosarcoma cell lines. Data taken from the Broad Institute CCLE (2019) section of cBioPortal. **E,** Survival probability of patients having high and low median expression of the "2c general" gene signature ($n = 38$), as represented by Kaplan–Meier plot. Patients with sarcoma were stratified on the basis of the optimal cut-off point. **F,** Survival probability of patients having high and low median expression of the "2c proteotoxic stress" gene signature ($n = 18$), as represented by Kaplan–Meier plot. Patients with sarcoma were stratified on the basis of the optimal cut-off point.

rapid accumulation of polyubiquitylated proteins (16, 28) and the appearance of endoplasmic reticulum stress, as evidenced by eIF2α phosphorylation (**Fig. 2C**). The proteolytic processing of eIF2α later on further confirms the activation of caspases in 2c-treated cells (32). Dose-dependent studies confirmed the induction of proteotoxic stress by 2c, as testified by the accumulation of polyubiquitylated proteins and of NOXA/PMAIP1 (Supplementary Fig. S3).

Interestingly, after 2c treatment, the apoptotic protein DIABLO/SMAC accumulates as a higher molecular weight form. DIABLO/SMAC is a mitochondrial protein released into the cytoplasm during apoptosis. When imported into the mitochondria, it is processed by the inner membrane peptidase complex to generate the mature form (33). Hence, the accumulation of the DIABLO/SMAC precursor in cells treated with 2c is indicative of defects in the import machinery, possibly because of an early induction of the mitochondrial unfolded protein response (34). In fact, the analysis of the mitochondria network, using anti-DIABLO/SMAC and anti-ATP synthase (β subunit) antibodies, evidenced an early and dramatic fragmentation of mitochondria in response to 2c (**Fig. 2D**). *In vivo* time-lapse confocal microscopy confirmed the rapid (within 1 hour) induction of mitochondrial fission by 2c (Supplementary videos S1 and S2).

Sub-mitochondrial clusters of DIABLO/SMAC are perturbed by 2c treatment

To gain insight into the structural changes of the mitochondrial network in response to 2c, we used STED superresolution microscopy, which provides an optical resolution below the diffraction limit (35). The β subunit of the ATP synthase, a subunit of the multiprotein complex localized in the mitochondrial inner membrane, including the cristae, was selected to visualize mitochondria (36). We also analyzed DIABLO/SMAC localization, which maturation is under 2c influence. Confocal and STED images are shown for comparison. Both leiomyosarcoma cell lines are characterized by elongated tubular mitochondria. The ATP synthase shows a relative homogeneous distribution, as described previously (35, 36). STED microscopy unveiled that DIABLO/SMAC localizes as small clusters, well separated and usually peripheral with respect to the ATP synthase (**Fig. 3**). Normalized fluorescence intensity profiles confirmed this distribution

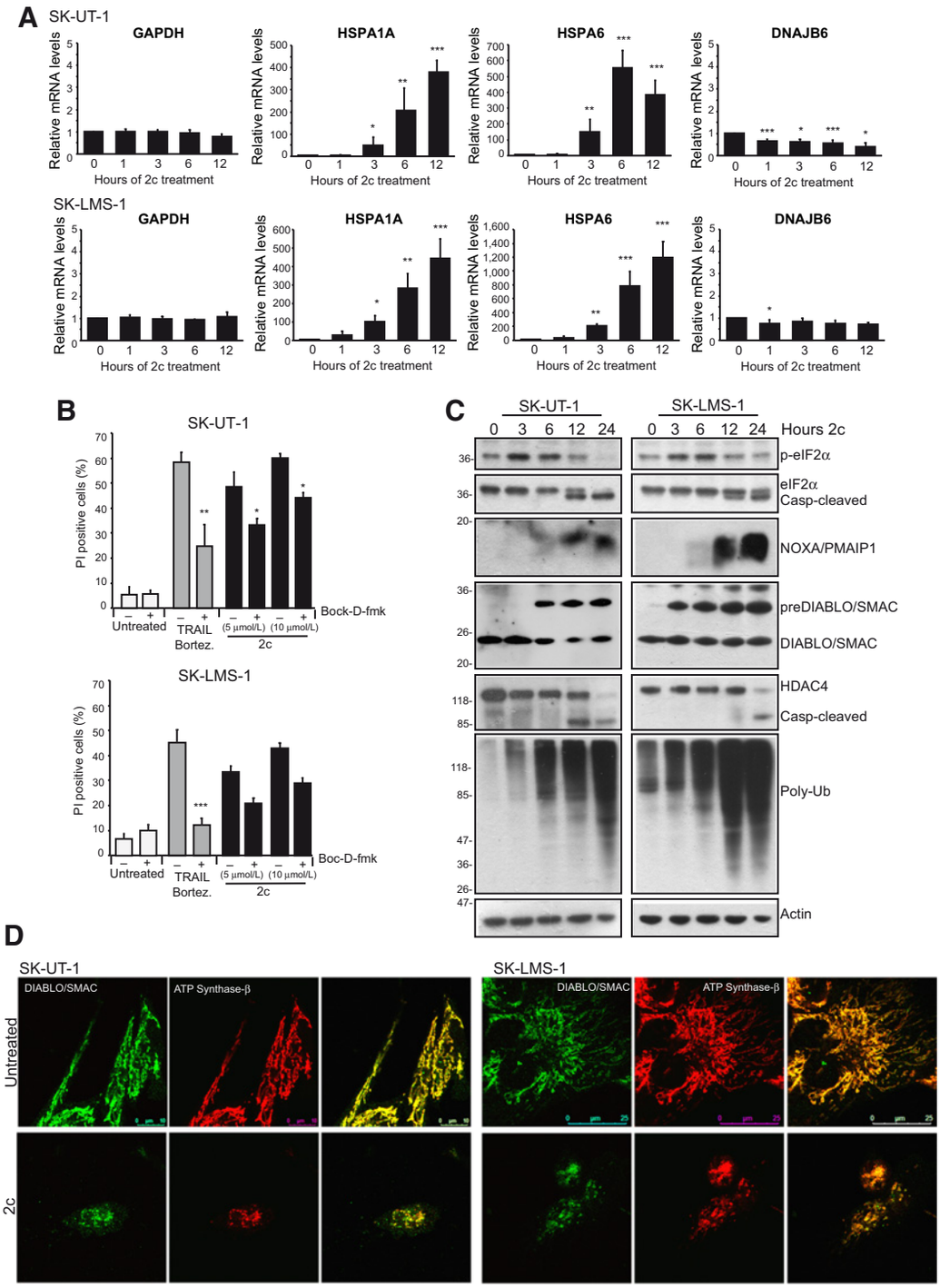

Figure 2.

2c triggers proteotoxic stress and cell death in leiomyosarcoma cells. **A,** qRT-PCR analysis of the mRNA levels of the indicated genes in SK-UT-1 or SK-LMS-1 cells treated with 10 μmol/L of 2c for the indicated times. **B,** SK-UT-1 and SK-LMS-1 cells were treated for 24 hours with the indicated concentrations of 2c or with a combination of TRAIL (2.5 ng/mL) and bortezomib (0.1 μmol/L). The broad caspase inhibitor Boc-D-fmk was used (50 μmol/L). Cell death was calculated as percentage of cells positive to PI staining. **C,** SK-UT-1 and SK-LMS-1 cells were treated with 2c (10 μmol/L) for the indicated times. Cellular lysates were generated and immunoblots were performed with the indicated antibodies. Actin was used as loading control. **D,** SK-UT-1 and SK-LMS-1 cells were treated or not with 10 μmol/L 2c for 4 hours. Immunofluorescence analysis was performed to visualize mitochondria morphology, using antibodies to visualize DIABLO/SMAC (green) and ATP synthase-β subunit (red). Confocal images are shown in pseudocolors and were acquired with a Leica SP8 LSM.

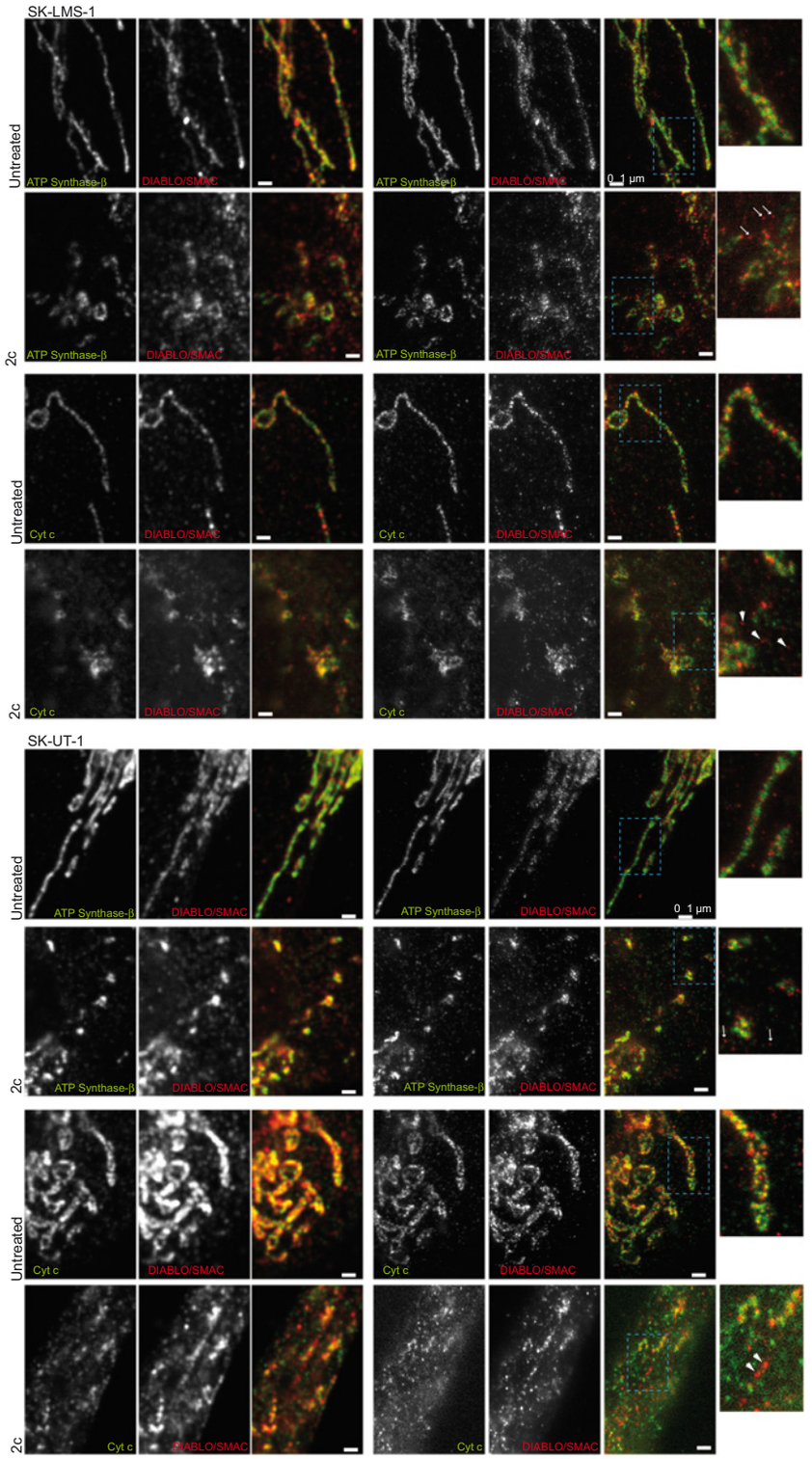

Figure 3.
STED superresolution microscopy of mitochondria under 2c-induced proteotoxic stress. Dual-color confocal and STED images of SK-UT-1 and SK-LMS-1 cells decorated with antibodies against ATP-synthase-β subunit (green)/DIABLO/SMAC (red) or with CytC (green)/DIABLO/SMAC (red). Cells were untreated or treated with 5 µmol/L of 2c for 4 hours. A single optical section is shown. Magnification was applied to the boxed areas. Bar = 1 µm.

(Supplementary Fig. S4). The peripheral localization of DIABLO/SMAC with respect to the ATP synthase-β is expected, because of the different compartmentalization of the two proteins. Overall, the described patterns of mitochondrial localization are similar in the two leiomyosarcoma cell lines.

2c induces a dramatic mitochondrial fragmentation. The 2D STED analysis in 2c-treated cells evidences that some DIABLO/SMAC clusters appear very distant from the ATP synthase domains (**Fig. 3** arrows). This observation is confirmed by the analysis of the fluorescence intensity profiles (Supplementary Fig. S4). The origin of these

distal DIABLO/SMAC clusters is unclear. They could represent the accumulation of the cytosolic precursor form of DIABLO/SMAC. To further understand the mitochondrial alterations triggered by 2c, we performed the STED colocalization analysis of CytC and DIABLO/SMAC, two proteins released into the cytoplasm from the intermembrane space during apoptosis. In untreated cells, separated clusters as well as partially colocalized clusters of CytC and DIABLO/SMAC can be observed (**Fig. 3**). In response to 2c, some partially colocalized clusters of CytC and DIABLO/SMAC persist. In parallel, DIABLO/SMAC clusters at a certain distance from small CytC spots appear (**Fig. 3** arrowheads in the magnification). A similar behavior is observed in the two leiomyosarcoma cells. Normalized fluorescence intensity profiles confirmed these different distributions (Supplementary Fig. S4). All the results were verified by reverting the secondary antibodies labeling (Supplementary Fig. S5 and S6).

In summary, this analysis demonstrates the existence of specific mitochondrial clusters of DIABLO/SMAC and that 2c triggers a profound reorganization of the mitochondrial network and of these clusters.

Optimization of 2c prodrug delivery in leiomyosarcoma cells

2c is poorly soluble in aqueous solutions, a limitation for its use *in vivo*. Recently, we have developed a prodrug version of 2c (2cPE), by using the PEG as a carrier. PEG promotes its solubility and improves the delivery (**Fig. 4A**). An ester linkage allows the release of active 2c from 2cPE, as operated by the secreted esterase PLA2G7 (28). To test the antitumoral potency of 2cPE *in vivo* against leiomyosarcomas, we first evaluated its ability to trigger cell death in leiomyosarcoma cells. Surprisingly, 2cPE is unable to trigger cell death in SK-UT-1 and SK-LMS-1 cells. The failure of 2cPE was further confirmed in DMR cells, another leiomyosarcoma cell line (**Fig. 4B**).

Peptide sequences cleaved by proteases have been utilized as bioactive linkers for the targeted delivery of specific drugs (37). The tumor microenvironment is characterized by increased levels of proteolytic activities, which promote tumor growth and invasion. Prodrug maturation, by tumor microenvironment proteases, could reduce off-target effects of a compound. Hence, we decided to adopt a new strategy to develop a new prodrug version of 2c. To increase its solubility and to specifically generate the active 2c at the tumor site, the compound was conjugated to PEG through a peptide linker. We selected a simple peptide linker constituted by the 3 aa Leu-Gly-Gly (LGG), a sequence that can be cleaved by different proteases secreted in the tumor microenvironment. **Figure 4C** illustrates the different proteases capable of processing the selected sequence and underlines the different sites. As expected, several cathepsins but also metalloproteinases are predicted to cleave the designed sequence. Several of the LGG proteases, particularly the matrix metalloproteinase *ADAM10* and *ADAMTS5*, are highly expressed in leiomyosarcomas (**Fig. 4D**). Curiously, leiomyosarcomas heterogeneously express *PLA2G7*. It is highly plausible that the group of leiomyosarcomas characterized by elevated levels of *PLA2G7* are those characterized by immune/inflammatory cells infiltrates (22). In fact, it is well known that inflammatory cells, including macrophages, express high levels of *PLA2G7* (38). Next, we investigated the expression levels of the putative LGG proteases in the two leiomyosarcoma cell lines. *CTSZ, CTSB, CTSL, CTSA, CTSD*, and *MMP2* are the most expressed proteases in SK-LMS-1 cells. The same group of cathepsins are also highly expressed in SK-UT-1 cells. In these cells the matrix metalloproteinase more abundantly expressed is *ADAM10*, which is also highly expressed in tumors (**Fig. 4E**). An important difference between tumors and cell lines regards the matrix metalloproteinases. In general, they are more abundantly expressed in tumors. It is possible that this difference stems from the presence of an activated stroma (39). The absence of *PLA2G7* expression in both cell lines explains the unresponsiveness to 2cPE treatment.

Generation of the protease-activated prodrug 2cPP

The main goal of this study is to test a new therapeutic strategy against leiomyosarcomas. Having confirmed that leiomyosarcomas express a repertoire of extracellular proteases capable of processing the sequence LGG, we decided to insert this sequence between the 2c and the PEG carrier.

The cleavage of the peptide sequence, connecting 2c to PEG can expose a negatively charged carboxy-terminus or a positively charged amino-terminus, depending on the orientation of the peptide sequence. To evaluate the effect of the negative and of the positive charges linked to 2c, we synthetized two variants of 2c: DU-DC2 with the exposed COO^- and DU-MS1 with a terminal NH_3^+ (**Fig. 5A**). When the ability to trigger cell death of the two compounds was compared respect to 2c, DU-DC2 resulted slightly less potent (**Fig. 5B**). It is possible that the introduced negative charge interferes with the cellular uptake of the 2c derivative and particularly with the interaction with the membrane. Although further studies are necessary to prove this hypothesis, we decided to introduce the LGG sequence with the orientation that will generate, after the proteolytic cleavage, the exposition of the NH_3^+ group. The new prodrug version was synthetized and named 2cPP (2c-protease–activated PEG-conjugated) and the structure is shown is **Fig. 5C**. The new molecule contains a diaminopropane linker that joins 2c to the LGG sequence and a D-alanine linker for the connection to the PEG moiety.

When leiomyosarcoma cell lines were treated with 2cPP, they all underwent cell death (**Fig. 5D**). The percentage of cell death is comparable with 2c treatment, with a slightly reduced potency of 2cPP. It is unclear whether this reduced *in vitro* potency is caused by a delay in the generation of the active drug, because of the protease-mediated processing. Similarly to 2c, 2cPP triggered cell death is partially dependent on caspase activation (**Fig. 5E**).

Induction of proteotoxic stress reduces tumor formation *in vivo*

To prove the antitumor efficiency of the new prodrug 2cPP *in vivo* against leiomyosarcomas, we selected SK-UT-1 cells that are able to efficiently process the prodrug in culture and show an aggressive growth *in vivo*. To exclude general toxicity, we initially evaluated the 2c and 2cPP against HUtSMCs, which represent the normal counterpart of SK-UT-1 cells. Cells were treated with the compounds and after 24 hours cell death was scored. 2c induces cell death with much lower efficiency in HUtSMC cells compared with SK-UT-1 (**Fig. 6A**). Most importantly, 2cPP was totally ineffective. Next, we compared the induction of proteotoxic stress by analyzing eIF2α phosphorylation and NOXA/PMAIP1 upregulation (**Fig. 6B**). HUtSMC show a lower level of basal eIF2α phosphorylation compared with SK-UT-1 cells. Hence, a higher proteotoxic stress seems to characterize cancer cells, as confirmed by the increased expression of *HSF1* in the two leiomyosarcoma cell lines compared with normal cells (Supplementary Fig. S7). Nevertheless, HUtSMC cells promptly augment eIF2α phosphorylation in response to 2c. In contrast, NOXA/PMAIP1 is upregulated only in SK-UT-1 cells. Therefore, normal cells seem to be protected from the vicious cycle of the proteotoxic stress–induced

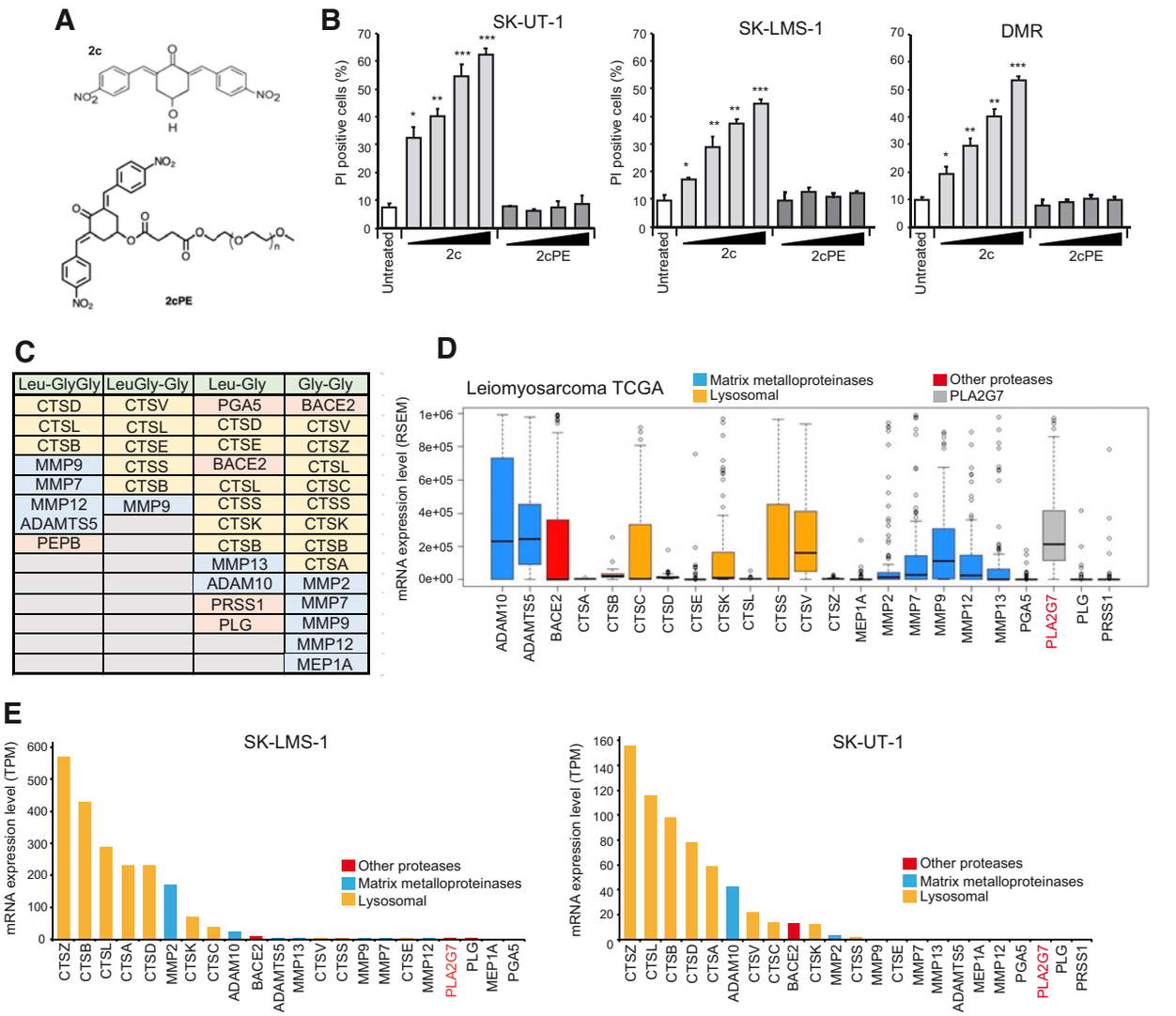

Figure 4.

Generation of a new prodrug version of 2c. **A,** Molecular structure of 2c and of its prodrug version 2cPE. **B,** The three leiomyosarcoma cell lines were treated for 24 hours with the increased concentrations of 2c or 2cPE (1/2.5/5/10 μmol/L). Cell death was calculated as percentage of cells positive to PI staining. **C,** List of the different proteases capable of cleaving the LGG sequence at the indicated sites as downloaded from MEROPS, the peptidase database (https://www.ebi.ac.uk/merops). Lysosomal proteases are in orange, metalloproteinases in light blue, other proteases in pink. **D,** Box plot representing mRNA expression levels (RSEM data) of LGG peptidases identified through MEROPS in patients with leiomyosarcomas ($n = 99$). Data were obtained from the whole Sarcoma dataset (TCGA, PanCancer Atlas; $n = 255$). Lysosomal proteases are in orange, metalloproteinases in light blue, other proteases in pink and PLA2G7 is identified in gray. **E,** mRNA expression levels (TPMs) of LGG peptidases identified through MEROPS in SK-UT-1 and SK-LMS-1 cell lines. Data were obtained from the database of the CCLE. Lysosomal proteases are in orange, metalloproteinases in light blue, other proteases in pink, and *PLA2G7* is identified in gray.

apoptosis. In HUtSMC, 2cPP is unable to trigger eIF2α phosphorylation, thus confirming its inactivity. This result suggests that normal cells are unable to efficiently generate the active drug by proteolytic processing.

Next, SK-UT-1 xenografts were generated in immunocompromised mice, and when the tumors reached the size of 0.1 cm^3, 2cPP (170 mg/kg) was administered intravenously, three times with 4-day intervals. This dose, considering the *in vitro* data, should correspond to approximately 11 mg/kg of the active compound. Alternatively, mice were treated with vehicle alone. 2cPP significantly inhibits tumor growth compared with control (**Fig. 6C**). The percentage of tumor growth inhibition (TGI) is 97.6% after 2 days from the first injection and the final TGI is 80.4%, compared with vehicle-treated animals. As expected from this analysis, tumors from 2cPP-treated mice weigh much less compared with those from vehicle-treated mice (**Fig. 6D**). No gross toxicity was observed and 2cPP does not induce any behavioral change or grossly visible pathologic changes. In the treated group, two mice show slight body weight loss (2.5%) and only a mouse evidenced a loss > 5% during the first week. This animal promptly recover weight during

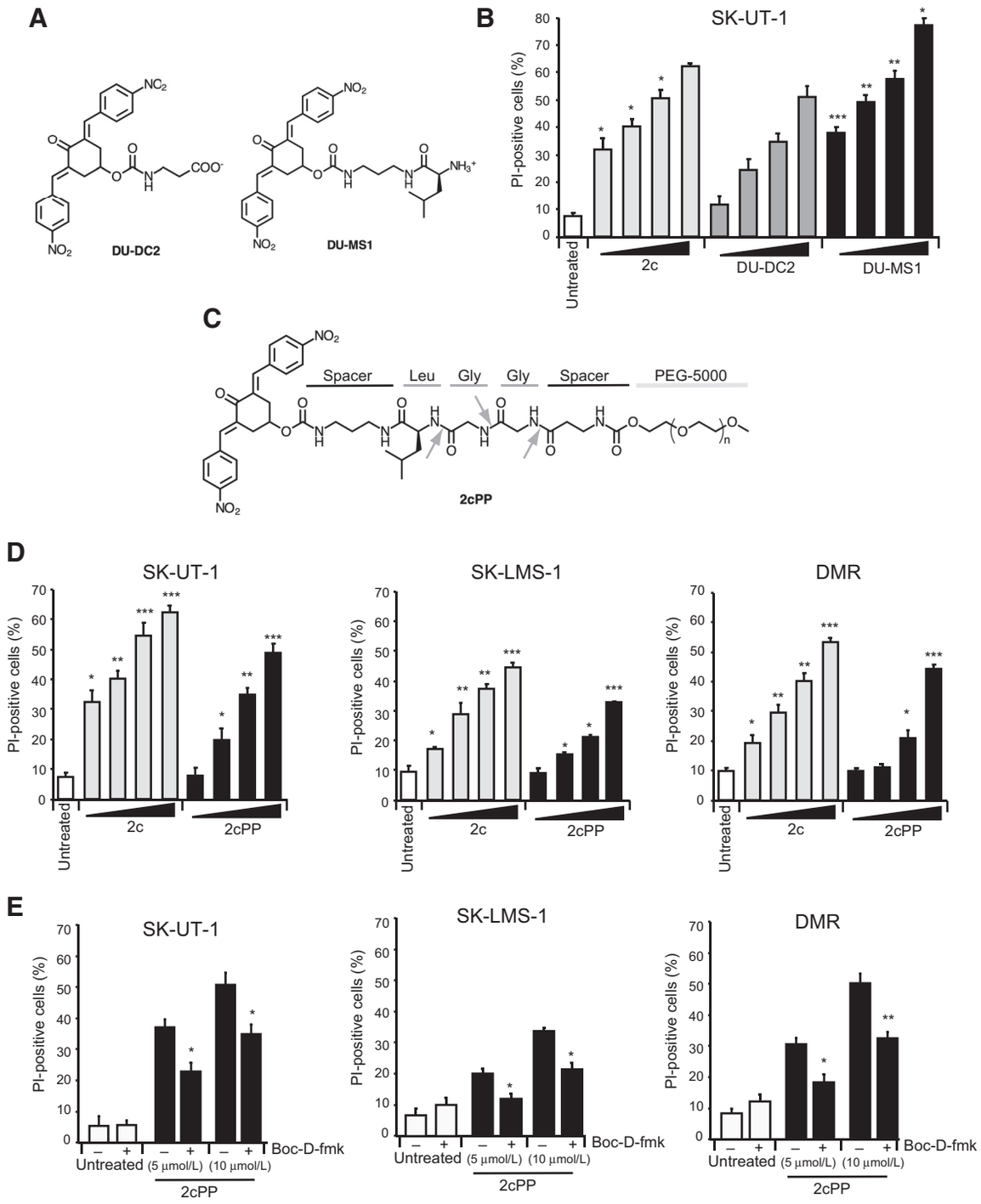

Figure 5.

Generation of the protease-activated prodrug 2cPP. **A,** Molecular structure of the new derivates of 2c with negative (DU-DC2) and positive (DU-MS1) charge. **B,** SK-UT-1 cells were treated for 24 hours with the increased concentrations of 2c, DU-DC2, or DU-MS1 (1/2.5/5/10 μmol/L). Cell death was calculated as percentage of cells positive to PI staining. **C,** Molecular structure of the new prodrug version of 2c (2cPP). Arrows indicate the possible sites of cleavage. Spacers and PEG are also indicated. **D,** The three leiomyosarcoma cell lines were treated for 24 hours with the increased concentrations of 2c or 2cPP (1/2.5/5/10 μmol/L). Cell death was calculated as percentage of cells positive to PI staining. **E,** The three leiomyosarcoma cell lines were treated for 24 hours with the indicated concentrations of 2cPP. The broad caspase inhibitor Boc-D-fmk was used (50 μmol/L). Cell death was calculated as percentage of cells positive to PI staining.

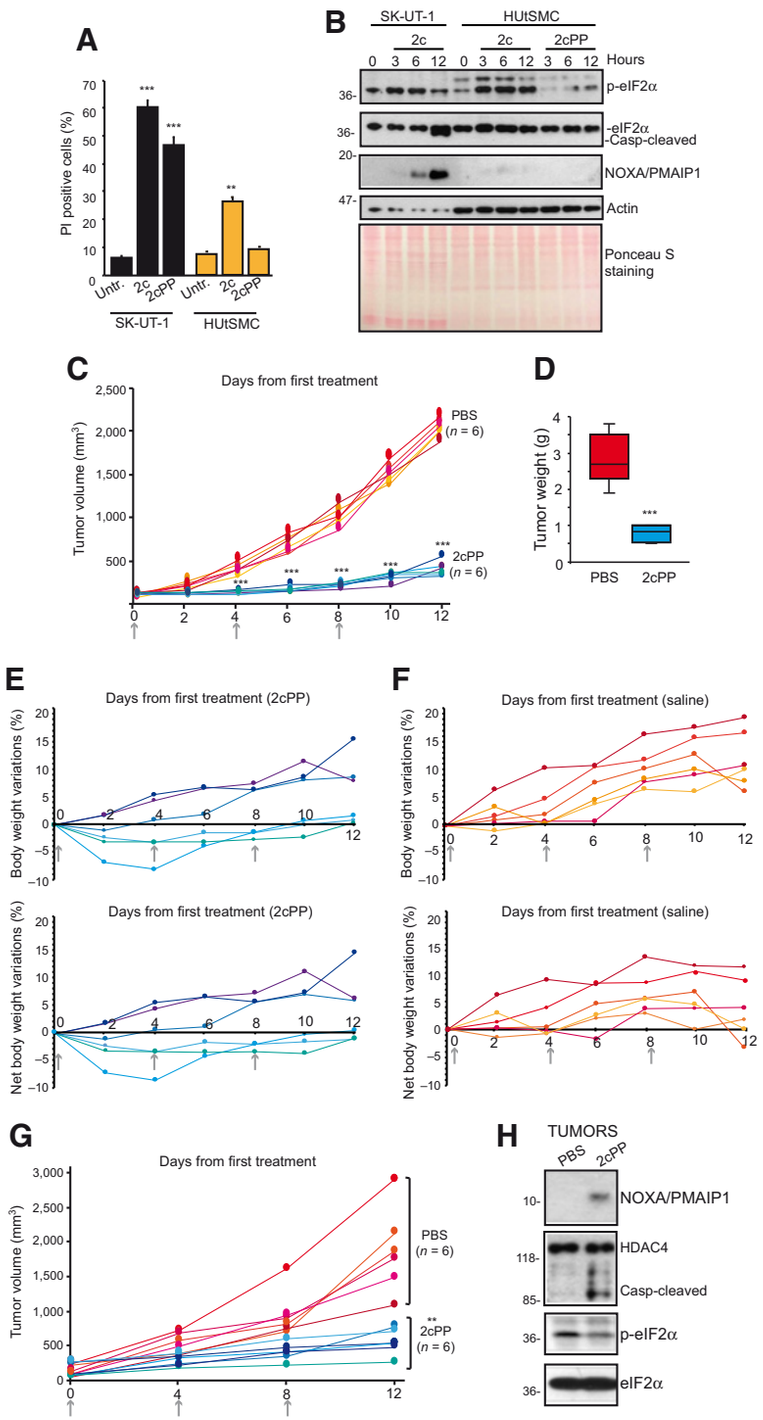

Figure 6.

Antitumor activity of 2cPP *in vivo*. **A,** HUtSMC and SK-UT-1 cells were treated for 24 hours with (10 μmol/L) of 2c or 2cPP. Cell death was calculated as percentage of cells positive to PI staining. **B,** HUtSMC and SK-UT-1 cells were treated with 2c (10 μmol/L) for the indicated times. Cellular lysates were generated and immunoblots were performed with the indicated antibodies. Ponceau S staining was included as loading control. **C,** Variations of SK-UT-1 leiomyosarcoma xenografts volume in mice following intravenous treatments with 2cPP (170 mg/kg) or a saline solution. Arrows indicate the injections. **D,** At day 12, tumors were dissected and final tumor weights measured. Mean tumor weights ± SD. **E,** Total body weights or net body weights (obtained by subtracting tumors) of mice treated with 2cPP, during xenograft studies with SK-UT-1 cells. Data are show as variations (%) relative to time 0. Arrows indicate the injections. **F,** Total body weights or net body weights (obtained by subtracting tumors) of mice treated with saline, during xenograft studies with SK-UT-1 cells. Data are show as variations (%) relative to time 0. Arrows indicate the injections. **G,** Variations of DMR leiomyosarcoma xenografts volume in mice following intravenous treatments with 2cPP (170 mg/kg) or a saline solution. Arrows indicate the injections. **H,** Immunoblot analysis using the indicated antibodies in xenografted tumors treated or not with 2cPP. Twenty-four hours after the last injection with 2cPP (170 mg/kg) or PBS alone, mice were sacrificed for the generation of tumor extracts.

the second week (**Fig. 6E**). Because of the strong TGI exhibited by 2cPP, tumors do not influence body weight of treated mice (compare body weight and net body weight variations). In contrast, in control mice tumor growth profoundly influences body weight (**Fig. 6F**). Next, we validated the potent antitumor activity of 2cPP in a second xenograft model of leiomyosarcomas using DMR cells. 2cPP was again efficient in blocking tumor growth (**Fig. 6H**). Immunoblot analysis confirmed the upregulation of NOXA/PMAIP1 and the induction of apoptosis, testified by HDAC4 cleavage, detectable only in tumors from 2cPP-treated mice (**Fig. 6G**). As observed above *in vitro* for SK-UT-1 (**Fig. 2**), after 24 hours from 2cPP injection eIF2α phosphorylation is exhausted.

In conclusion, augmenting proteotoxic stress in leiomyosarcoma cells exerts a strong antitumor activity *in vivo*.

Discussion

In this article, we have proved that raising proteotoxic stress can trigger cell death in leiomyosarcoma cells and reduce tumor growth *in vivo*. We have shown that aggressive leiomyosarcomas have an intrinsic higher level of proteotoxic stress, a condition that could render these tumors uncapable of managing further increases of proteotoxic stress.

Induction of proteotoxic stress is emerging as a new therapeutic option and compounds capable of enhancing proteotoxic stress are under investigation (8–10, 40–42). The main targets of these small molecules are the chaperone system and the ubiquitin-proteasome system (UPS; ref. 10). 2c belongs to the family of diaryldienone derivatives, small molecules able to alkylate various cellular nucleophiles and cysteines in particular (13, 16, 42). 2c is a nonselective inhibitor of the UPS because it reacts with the catalytic cysteines of deubiquitylases (16, 28). Further studies have shown that 2c can react also with cysteines exposed at the surface of several proteins (17). Hence, these compounds can elicit proteotoxic stress directly, through the alteration of protein folding and indirectly, by blocking the UPS (17, 43, 44). Diaryldienone derivatives can also affect the transport of misfolded proteins and aggresome formation, (45) and can reduce glutathione levels (46), thus inducing oxidative stress (43, 44). Mitochondrial functions are strongly affected by these compounds (25, 44). From all these dysfunctions, proteotoxic stress become unmanageable and ultimately cell death occurs.

DIABLO/SMAC is a mitochondrial proapoptotic protein, whose maturation is influenced by 2c-induced proteotoxic stress. DIABLO/SMAC is released into the cytosol and promotes caspase activities by inhibiting the inhibitors of apoptosis (IAP). DIABLO/SMAC maturation, as operated by the mitochondrial rhomboid protease PARLn, generates the amino-terminal IAP-binding motif (33). Few data are available on DIABLO/SMAC mitochondrial localization. By using two-color STED microscopy, we have defined that DIABLO/SMAC exists in the intermembrane mitochondrial space as demarcated clusters, partially colocalizing with CytC and distinct from ATP synthase-β. The organization in clusters was observed also for other mitochondrial proteins (36). In its mature form, DIABLO/SMAC acts as a tetramer to bind IAPs (47). Its status when sequestered into the mitochondria is unclear. Our data suggest that specific sub-mitochondrial domains enriched for DIABLO/SMAC exist. Interestingly, CytC can partially colocalize with DIABLO/SMAC clusters and CytC can localize also in the cristae (48). Whether these colocalizing clusters represent mitochondrial cristae deserves further studies. Importantly, in 2c-treated cells, a dramatic mitochondrial fragmentation occurs and small spots of DIABLO/SMAC appear. Because they appear very early and much earlier than caspase activation, it is improbable that these spots represent the mature form of DIABLO/SMAC released from the mitochondria. Instead, because dysfunctions in the import of mitochondrial proteins occur early in response to proteotoxic stress, (34) they could represent the cytosolic DIABLO/SMAC precursor.

To potentiate the antineoplastic activity of 2c, we have generated 2cPP, a prodrug version that should be activated in the tumor microenvironment. 2cPP is inactive in its native state and gain high potency immediately after proteases release the active 2c. The designed sequence LGG can be cleaved by different peptidases, including lysosomal cathepsins and certain metalloproteases, two families of proteases abundantly secreted in the tumor microenvironment (39, 49). By linking 2c to PEG through a peptide, we have resolved the poor solubility of the compound, increased the specificity of action and reduced the general toxicity. As final cleaved product 2c, through the diaminopropane linker maintains a Lys. This additional structure only partially influences the pro-death activity of 2c *in vitro*. Different approaches to generate amino acid or peptide-conjugated drugs have been exploited (37). Interestingly, pioneering studies demonstrated that a Leu–doxorubicin prodrug shows higher antitumor efficiency *in vivo* when compared with the parental drug (50).

Overinduction of proteotoxic stress can be deleterious also for normal cells. In uterine smooth-muscle cells, high doses of 2c can trigger cell death, although at much reduced extent compared with leiomyosarcoma cells. Importantly, the insertion of the protease sensitive linker further reduces the toxic effect of 2c against normal cells. Uterine smooth muscle cells are not influenced by 2cPP and mice treated with 2cPP do not evidence signs of toxicity. The strong antitumor activity of 2cPP against leiomyosarcoma cells *in vivo* demonstrates that the induction of proteotoxic stress can be a valid option to treat these malignant tumors.

Although we have focused the study on leiomyosarcomas, our discoveries can also be applied to other tumors where proteotoxic stress is elevated. Moreover, because we have selected a simple aa sequence for prodrug delivery, it is highly plausible that a set of proteases capable of activating 2cPP is present in the microenvironment of different tumors.

Authors' Disclosures

G. Grignani reports other support from Eisai, Lilly, Bayer, Novartis, Merck, and Glaxo Smith Kline outside the submitted work. F. Benedetti reports grants from POR-FESR Regione Friuli-Venezia Giulia, project ATeNA, during the conduct of the study. C. Brancolini reports grants from Sarcoma Foundation of America, POR-FESR Regione Friuli-Venezia Giulia project ATeNA, FPRC 5 × 1000 Ministero della Salute 2015 ImGen, and AIRC IG 23104 during the conduct of the study. No disclosures were reported by the other authors.

Authors' Contributions

L. Iuliano: Data curation, validation, investigation. **S. Drioli:** Resources, validation, methodology. **Y. Pignochino:** Data curation, investigation. **C.M. Cafiero:** Resources, investigation. **M. Minisini:** Investigation. **F. D'Este:** Resources, data curation, methodology. **R. Picco:** Data curation, formal analysis. **E. Dalla:** Data curation, formal analysis. **G. Giordano:** Validation. **G. Grignani:** Supervision. **E. Di Giorgio:** Methodology. **F. Benedetti:** Conceptualization, supervision, funding acquisition. **F. Felluga:** Resources, investigation, methodology, writing–original draft. **C. Brancolini:** Conceptualization, resources, data curation, supervision, funding acquisition, visualization, writing–original draft.

Acknowledgements

This study was supported by POR-FESR Regione Friuli-Venezia Giulia project ATeNA, to F. Benedetti and C. Brancolini, FPRC 5 × 1000 Ministero della Salute 2015 ImGen and AIRC IG 23104 to G. Grignani; and by the Sarcoma Foundation of America, to C. Brancolini.

We thank Andrea Rasola for kindly providing Radicicol.

The costs of publication of this article were defrayed in part by the payment of page charges. This article must therefore be hereby marked *advertisement* in accordance with 18 U.S.C. Section 1734 solely to indicate this fact.

Received June 22, 2020; revised November 27, 2020; accepted March 9, 2021; published first March 30, 2021.

References

1. Duffaud F, Ray-Coquard I, Salas S, Pautier P. Recent advances in understanding and managing leiomyosarcomas. F1000Prime Rep 2015;7:55.
2. Gladdy RA, Qin L, Moraco N, Agaram NP, Brennan MF, Singer S. Predictors of survival and recurrence in primary leiomyosarcoma. Ann Surg Oncol 2013;20: 1851–57.
3. Chibon F, Darbo E, Pérot G. Leiomyosarcomas: whole genome sequencing for a whole biology characterization. Curr Opin Oncol 2019; 31:317–21.
4. Mäkinen N, Aavikko M, Heikkinen T, Taipale M, Taipale J, Koivisto-Korander R, et al. Exome sequencing of uterine leiomyosarcomas identifies frequent mutations in TP53, ATRX, and MED12. PLoS Genet 2016;12:e1005850.
5. Abeshouse A, Adebamowo C, Adebamowo SN, Akbani R, Akeredolu T, Ally A, et al. Comprehensive and integrated genomic characterization of adult soft tissue sarcomas. Cell 2017;171:950–65.
6. Seddon B, Strauss SJ, Whelan J, Leahy M, Woll PJ, Cowie F, et al. Gemcitabine and docetaxel versus doxorubicin as first-line treatment in previously untreated advanced unresectable or metastatic soft-tissue sarcomas (GeDDiS): a randomised controlled phase 3 trial. Lancet Oncol 2017;18:1397–410.
7. Tap WD, Wagner AJ, Schöffski P, Martin-Broto J, Krarup-Hansen A, Ganjoo KN, et al. Effect of doxorubicin plus olaratumab vs doxorubicin plus placebo on survival in patients with advanced soft tissue sarcomas: the ANNOUNCE randomized clinical trial. JAMA 2020;323:1266–76.
8. McConkey DJ. The integrated stress response and proteotoxicity in cancer therapy. Biochem Biophys Res Commun 2017;482:450–3.
9. Chui MH, Doodnauth SA, Erdmann N, Tiedemann RE, Sircoulomb F, Drapkin R, et al. Chromosomal instability and mTORC1 activation through PTEN loss contribute to proteotoxic stress in ovarian carcinoma. Cancer Res 2019;79:5536–49.
10. Guang MHZ, Kavanagh EL, Dunne LP, Dowling P, Zhang L, Lindsay S, et al. Targeting proteotoxic stress in cancer: a review of the role that protein quality control pathways play in oncogenesis. Cancers 2019;11:66.
11. Ohashi A, Ohori M, Iwai K, Nakayama Y, Nambu T, Morishita D, et al. Aneuploidy generates proteotoxic stress and DNA damage concurrently with p53-mediated post-mitotic apoptosis in SAC-impaired cells. Nat Commun 2015; 6:7668.
12. Brancolini C, Iuliano L. Proteotoxic stress and cell death in cancer cells. Cancers 2020;12:2385.
13. Coughlin K, Anchoori R, Iizuka Y, Meints J, MacNeill L, Voge RI, et al. Small-molecule RA-9 inhibits proteasome-associated DUBs and ovarian cancer in vitro and in vivo via exacerbating unfolded protein responses. Clin Cancer Res 2014; 20:3174–86.
14. Le Moigne R, Aftab BT, Djakovic S, Dhimolea E, Valle E, Murnane M, et al. The p97 inhibitor CB-5083 is a unique disrupter of protein homeostasis in models of multiple myeloma. Mol Cancer Ther 2017;16:2375–86.
15. Yu Y, Zhao Y, Fan Y, Chen Z, Li H, Lu J, et al. Inhibition of ubiquitin-specific protease 14 suppresses cell proliferation and synergizes with chemotherapeutic agents in neuroblastoma. Mol Cancer Ther 2019;18:1045–56.
16. Tomasella A, Picco R, Ciotti S, Sgorbissa A, Bianchi E, Manfredini R, et al. The isopeptidase inhibitor 2cPE triggers proteotoxic stress and ATM activation in chronic lymphocytic leukemia cells. Oncotarget 2016;7:45429–43.
17. Ciotti S, Sgarra R, Sgorbissa A, Penzo C, Tomasella A, Casarsa F, et al. The binding landscape of a partially-selective isopeptidase inhibitor with potent pro-death activity, based on the bis(arylidene)cyclohexanone scaffold. Cell Death Dis 2018;9:184.
18. Di Giorgio E, Clocchiatti A, Piccinin S, Sgorbissa A, Viviani G, Peruzzo P, et al. MEF2 is a converging hub for histone deacetylase 4 and phosphatidylinositol 3-kinase/Akt-induced transformation. Mol Cell Biol 2013;33: 4473–91.
19. Cerami E, Gao J, Dogrusoz U, Gross BE, Sumer SO, Aksoy BA, et al. The cBio cancer genomics portal: an open platform for exploring multidimensional cancer genomics data. Cancer Discov 2012;2:401–4.
20. Cancer Genome Atlas Research Network; Weinstein JN, Collisson EA, Mills GB, Shaw KRM, Ozenberger BA, et al. The cancer genome atlas pan-cancer analysis project. Nat Genet 2013;45:1113–20.
21. Ghandi M, Huang FW, Jané-Valbuena J, Kryukov GV, Lo CC, McDonald ER 3rd, et al. Next-generation characterization of the Cancer Cell Line Encyclopedia. Nature 2019;569:503–8.
22. Di Giorgio E, Paluvai H, Picco R, Brancolini C. Genetic programs driving oncogenic transformation: lessons from *in vitro* models. Int J Mol Sci 2019; 20:6283.
23. Dardis C. survMisc: Miscellaneous Functions for Survival Data, R Package Version: 0.5.5; 2018. Available from: https://CRAN.R-project.org/package=survMisc.
24. Sgorbissa A, Tomasella A, Potu H, Manini I, Brancolini C. Type I IFNs signaling and apoptosis resistance in glioblastoma cells. Apoptosis 2011;16: 1229–44.
25. Fontanini A, Foti C, Potu H, Crivellato E, Maestro R, Bernardi P, et al. The isopeptidase inhibitor G5 triggers a caspase-independent necrotic death in cells resistant to apoptosis: a comparative study with the proteasome inhibitor bortezomib. J Biol Chem 2009;284:8369–81.
26. Tomasella A, Blangy A, Brancolini C. A receptor-interacting protein 1 (RIP1)-independent necrotic death under the control of protein phosphatase PP2A that involves the reorganization of actin cytoskeleton and the action of cofilin-1. J Biol Chem 2014;289:25699–710.
27. Paroni G, Mizzau M, Henderson C, Del Sal G, Schneider C, Brancolini C. Caspase-dependent regulation of Histone Deacetylase 4 nuclear-cytoplasmic shuttling promotes apoptosis. Mol Biol Cell 2004;15:2804–18.
28. Cersosimo U, Sgorbissa A, Foti C, Drioli S, Angelica R, Tomasella A, et al. Synthesis, characterization, and optimization for *in vivo* delivery of a nonselective isopeptidase inhibitor as new antineoplastic agent. J Med Chem 2015;58: 1691–704.
29. Barretina J, Caponigro G, Stransky N, Venkatesan K, Margolin AA, Kim S, et al. The cancer cell line encyclopedia enables predictive modelling of anticancer drug sensitivity. Nature 2012;483:603–7.
30. Zhu J, Tsai HJ, Gordon MR, Li R. Cellular stress associated with aneuploidy. Dev Cell 2018;44:420–31.
31. Domcke S, Sinha R, Levine DA, Sander C, Schultz N. Evaluating cell lines as tumour models by comparison of genomic profiles. Nat Commun 2013;4: 2126.
32. Satoh S, Hijikata M, Handa H, Shimotohno K. Caspase-mediated cleavage of eukaryotic translation initiation factor subunit 2alpha. Biochem J 1999;342: 65–70.
33. Saita S, Nolte H, Fiedler KU, Kashkar H, Venne AS, Zahedi RP, et al. PARL mediates Smac proteolytic maturation in mitochondria to promote apoptosis. Nat Cell Biol 2017;19:318–28.
34. Andréasson C, Ott M, Büttner S. Mitochondria orchestrate proteostatic and metabolic stress responses. EMBO Rep 2019;20:e47865.
35. Donnert G, Keller J, Wurm CA, Rizzoli SO, Westphal V, Schönle A, et al. Two-color far-field fluorescence nanoscopy. Biophys J 2007;92:L67–9.
36. Jans DC, Wurm CA, Riedel D, Wenzel D, Stagge F, Deckers M, et al. STED super-resolution microscopy reveals an array of MINOS clusters along human mitochondria. Proc Natl Acad Sci U S A 2013;110:8936–41.
37. Poreba M. Protease-activated prodrugs: strategies, challenges, and future directions. FEBS J 2020;287:1936–69.
38. Low HB, Png CW, Li C, Wang DY, Wong SBJ, Zhang Y. Monocyte-derived factors including PLA2G7 induced by macrophage-nasopharyngeal carcinoma cell interaction promote tumor cell invasiveness. Oncotarget 2016;7: 55473–90.
39. Gonzalez-Avila G, Sommer B, García-Hernández AA, Ramos C. Matrix metalloproteinases' role in tumor microenvironment. Adv Exp Med Biol 2020;1245: 97–131.
40. Harris IS, Endress JE, Coloff JL, Selfors LM, McBrayer SK, Rosenbluth JM, et al. Deubiquitinases maintain protein homeostasis and survival of cancer cells upon glutathione depletion. Cell Metab 2019;29:1166–81.
41. Dias MH, Fonseca CS, Zeidler JD, Albuquerque LL, da Silva MS, Cararo-Lopes E, et al. Fibroblast growth factor 2 lethally sensitizes cancer cells to stress-targeted therapeutic inhibitors. Mol Oncol 2019;13:290–306.
42. Karki SS, Das U, Umemura N, Sakagami H, Iwamoto S, Kawase M, et al. 3,5-bis(3-alkylaminomethyl-4-hydroxybenzylidene)-4-piperidones: a novel class of potent tumor-selective cytotoxins. J Med Chem 2016;59: 763–9.
43. Ciotti S, Iuliano L, Cefalù S, Comelli M, Mavelli I, Di Giorgio E, et al. GSK3β is a key regulator of the ROS-dependent necrotic death induced by the quinone DMNQ. Cell Death Dis 2020;11:2.
44. Zhang X, Pellegrini P, Saei AA, Hillert EK, Mazurkiewicz M, Olofsson MH, et al. The deubiquitinase inhibitor b-AP15 induces strong proteotoxic stress and mitochondrial damage. Biochem Pharmacol 2018;156:291–301.
45. Hillert EK, Brnjic S, Zhang X, Mazurkiewicz M, Saei AA, Mofers A, et al. Proteasome inhibitor b-AP15 induces enhanced proteotoxicity by inhibiting cytoprotective aggresome formation. Cancer Lett 2019;448:70–83.

46. Foti C, Florean C, Pezzutto A, Roncaglia P, Tomasella A, Gustincich S, et al. Characterization of caspase-dependent and caspase-independent deaths in glioblastoma cells treated with inhibitors of the ubiquitin-proteasome system. Mol Cancer Ther 2009; 8:3140–50.
47. Mastrangelo E, Vachette P, Cossu F, Malvezzi F, Bolognesi M, Milani M. The activator of apoptosis Smac-DIABLO acts as a tetramer in solution. Biophys J 2015;108:714–23.
48. Scorrano L, Ashiya M, Buttle K, Weiler S, Oakes SA, Mannella CA, et al. A distinct pathway remodels mitochondrial cristae and mobilizes Cytochrome C during apoptosis. Dev Cell 2002;2:55–67.
49. Vidak E, Javoršek U, Vizovišek M, Turk B. Cysteine cathepsins and their extracellular roles: shaping the microenvironment. Cells 2019;8:264.
50. Breistøl K, Hendriks HR, Fodstad O. Superior therapeutic efficacy of N-L-leucyl-doxorubicin versus doxorubicin in human melanoma xenografts correlates with higher tumour concentrations of free drug. Eur J Cancer 1999;35:1143–49.